Modeling the Bias and Temperature Dependence of a C-Class MESFET Amplifier

Sagrario Muñoz, Jose L. Sebastián, and Juan D. Gallego, *Member, IEEE*

***Abstract*— In this paper, a complete bias and temperature-dependent large-signal model for a MESFET is determined from experimental S-parameters and dc measurements. This model is used in the analysis of the performance of a C-class amplifier at 4 GHz over a -50° to 100°C temperature range and for different bias conditions. The dependencies of the elements of the equivalent circuit, as well as the amplifier gain on the temperature and the operating point, are evaluated. The gain optimization and the analysis as a function of temperature of the MESFET amplifier are done by using the describing function technique. Optimum bias device conditions in the C-class are obtained for maximum gain and also the flattest gain versus input power rate. A comparison between theoretical and measured results over temperature and bias ranges is shown. Experimental results show an excellent agreement with the theoretical analysis.**

***Index Terms*—MESFET amplifiers, microwave amplifiers, microwave FET amplifiers.**

I. Introduction

GAAS MESFET's are presently one of the most common active devices used in microwave circuit design. Therefore, many authors have tried to develop accurate MESFET models. A complete nonlinear device model must take into account the different phenomena involved in the nonlinear behavior of the transistor, and in particular, a great effort must be made to analyze the influence of the bias operating point and temperature on a MESFET's behavior. In this paper, a small-signal model for NE71083 (width $=300$ μm, length $=0.3$ μm) is calculated at different bias conditions and within the temperature range -50 °C–100 °C. This model is used in the nonlinear analysis of a C-class MESFET RF amplifier. No attempt has been made to obtain a very high output power from the NE71083, as the interest of this paper is focused on the characterization of the bias and temperature dependence. For analysis of GaAs power amplifiers traditional methods, such as harmonic balance or load pulling, mainly consider room temperature device operation; thus, the determination of the optimum bias conditions for maximum gain at different temperatures are not easily achieved. In this paper, the nonlinear analysis of a C-class amplifier is performed using the describing function technique. Although the use of this technique has not been very extensive in RF circuits, due to its mathematical complexity, it leads to the appropriate design of the input and output matching networks and the particular bias condition for maximum gain. The experimental results obtained for the amplifier confirm the validity of the model and the suitability of the describing function technique in nonlinear analysis of microwave RF amplifiers.

Manuscript received June 18, 1996; revised December 24, 1996.

S. Muñoz and J. L. Sebastián are with the Facultad de Ciencias Físicas, U.C.M., 28040 Madrid, Spain.

J. D. Gallego is with Centro Astronómico de Yebes O.A.N., 19080 Guadalajara, Spain.

Publisher Item Identifier S 0018-9480(97)02527-1.

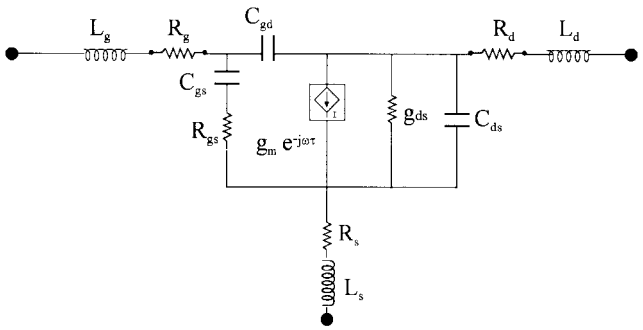

Fig. 1. Small-signal MESFET equivalent circuit.

The small-signal equivalent circuit parameter extraction method is based on dc and S-parameters' measurements. The main advantage of the method is that a small-signal model for each bias condition and temperature value is obtained from device characterization without requiring optimization. Large signal information is straightforwardly derived from the different small-signal models at different temperatures and bias.

Most of the work in the literature of C-class amplifier design was performed for bipolar transistors [1]. In this paper, a bias and temperature model is considered for the nonlinear analysis of a C-class amplifier. The bias conditions chosen in this paper are for a C-class operation to obtain higher efficiency. Experimental results show that the effect of temperature and bias conditions are of primary importance for explaining the overall performance of the C-class biased RF-power amplifier.

Section II of this paper describes dc and ac device characterization and the small-signal equivalent circuit parameter extraction method for each bias condition and temperature value. The nonlinear analysis of a C-class amplifier using the model obtained is discussed in Section III. Finally, the experimental results obtained for the amplifier designed within the considered bias and temperature ranges, along with the conclusions, are presented in Sections IV and V, respectively.

II. Transistor Modeling

In this section, the equivalent circuit element values of the model, shown in Fig. 1, are evaluated as a function of bias

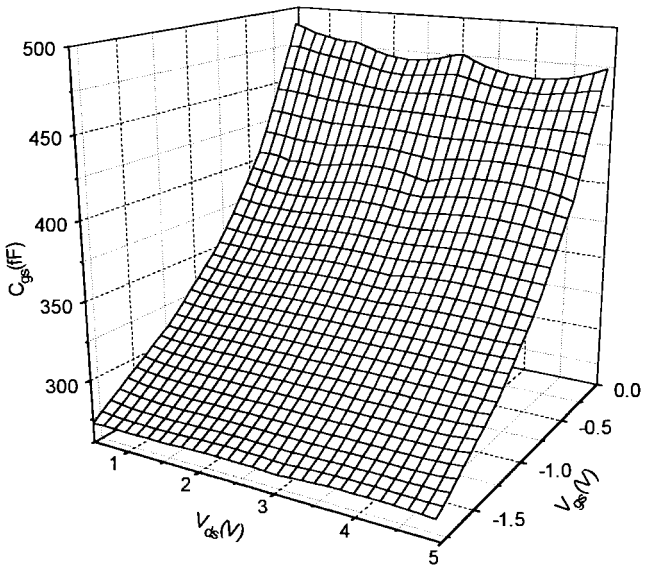

Fig. 2. C_{gs} as a function of the bias voltages.

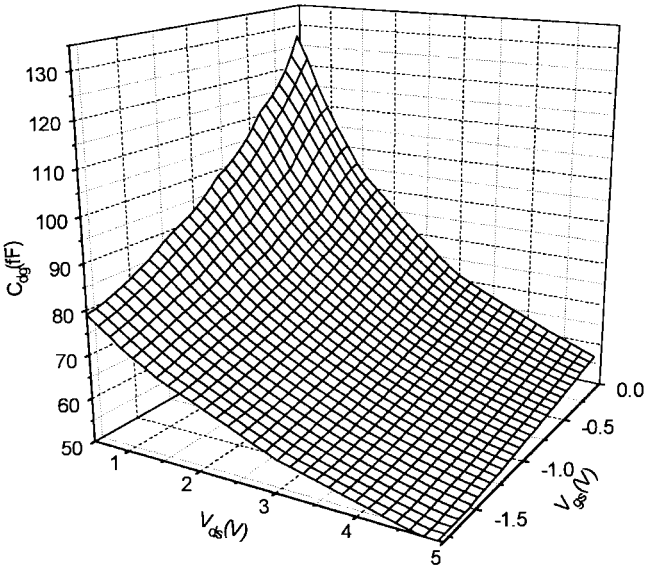

Fig. 3. C_{dg} as a function of the bias voltages.

conditions and temperature values. The reason for considering the bias and temperature dependencies of the element values is to obtain large-signal information. The MESFET model obtained is used for the design and analysis of a C-class amplifier.

For the small-signal model, shown in Fig. 1, conventional methods [2]–[4] are used for reliable determination of intrinsic and extrinsic elements. small-signal S-parameters' measurements are carried out by using a proper test fixture and a thru-reflect-line (TRL) *two tier* calibration [5].

S-parameters were measured from 1 to 26 GHz at a 100 bias point in the range $1 < V_{\rm ds} < 5$ V, $-1.8 < V_{\rm gs} < 0.2$ V.

For the dc measurements, the test fixture was terminated with two matched 50-Ω loads to avoid device oscillations.

For the particular bias range of $V_{\rm ds}$ and $V_{\rm gs}$ considered in this work, device capacitances are the main intrinsic parameters as g_m and $g_{\rm ds}$ have peculiar values (both very small).

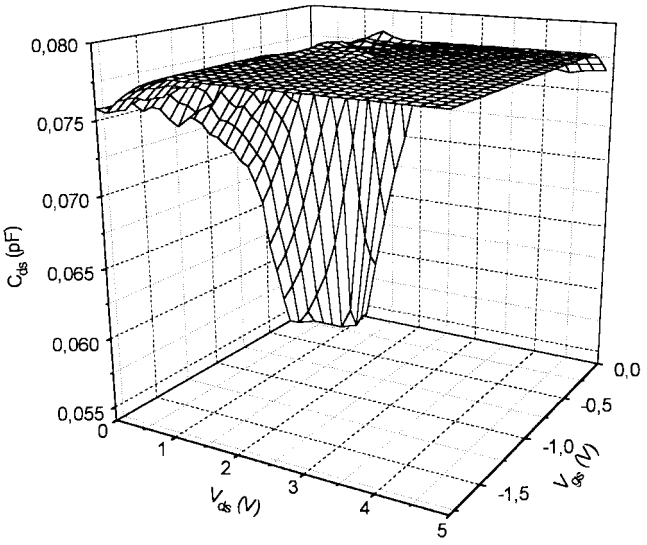

Fig. 4. $C_{\rm ds}$ as a function of the bias voltages.

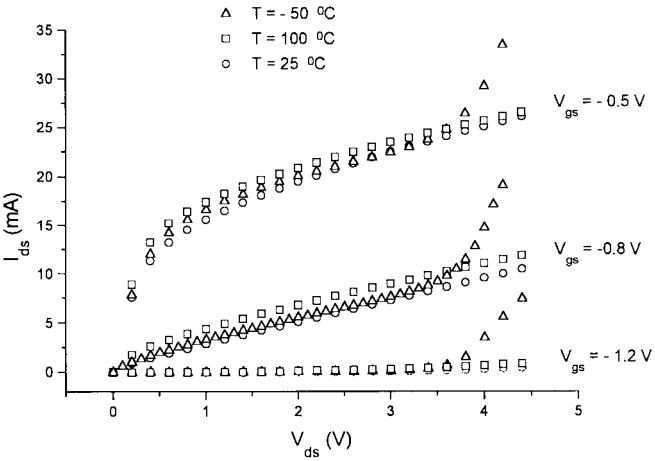

Fig. 5. Dc characteristics of NE71083 at -50 °C, 25 °C, and 100 °C.

A. Bias Dependence

Common MESFET models used in the saturated velocity regime are only accurate over a small range around the bias point. This is due to the fact that the device transconductance, drain–source conductance, and gate–source and gate–drain capacitances are bias-dependent and should be considered as point functions.

For the particular bias range considered in this paper (C-class), the intrinsic elements that show a more significant bias dependency are the gate–source and gate–drain capacitances as shown in Figs. 2 and 3 while the drain–source capacitance can be considered constant as shown in Fig. 4.

A good match to the experimental results is provided by the empirical expressions [6]

$$C_{\rm gs} = C_{\rm gs_0}\left\{\frac{\exp(A_1V_{\rm gs}) + A_2(V_{\rm gs}+V_{\rm ds})10^{A_3(V_{\rm gs}+V_{\rm ds})}}{1+A_4V_{\rm gs}10^{A_3V_{\rm gs}}}\right\} \tag{1}$$

$$C_{\rm dg} = C_{\rm dg_0}\left\{\frac{\exp(B_1V_{\rm ds}) + B_2(V_{\rm gs}+V_{\rm ds})10^{B_3(V_{\rm gs}+V_{\rm ds})}}{1+B_4V_{\rm ds}10^{B_3V_{\rm ds}}}\right\}. \tag{2}$$

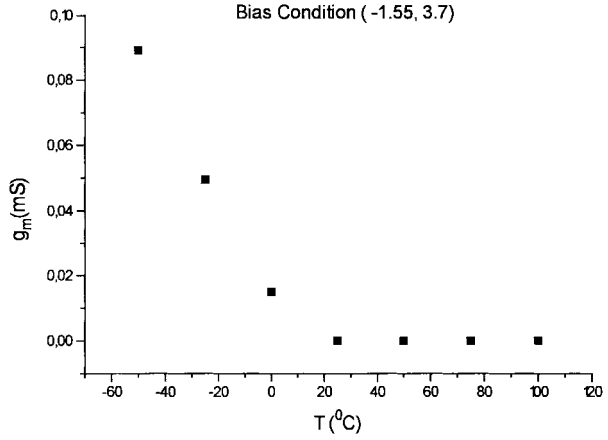

Fig. 6. g_m as a function of temperature.

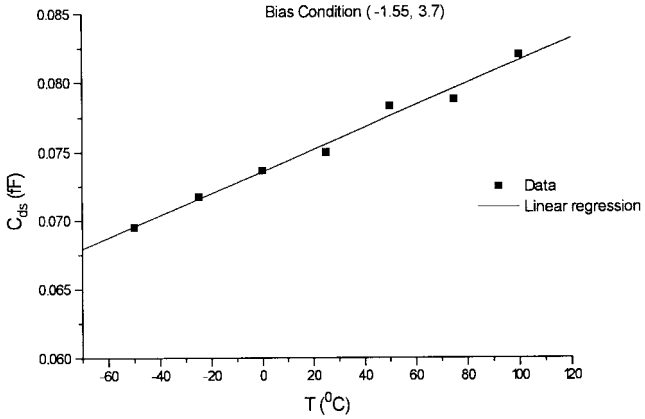

Fig. 7. $C_{\rm ds}$ as a function of temperature.

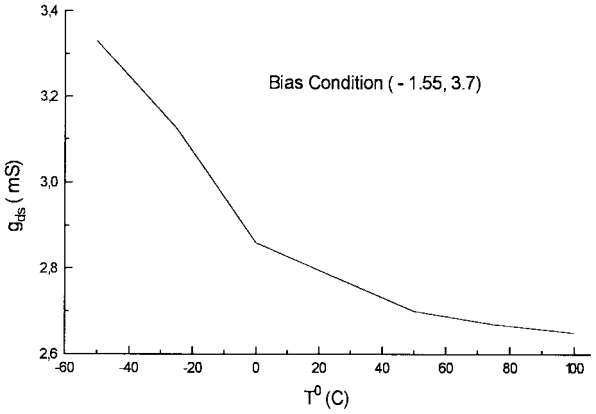

Fig. 8. $g_{\rm ds}$ as a function of temperature.

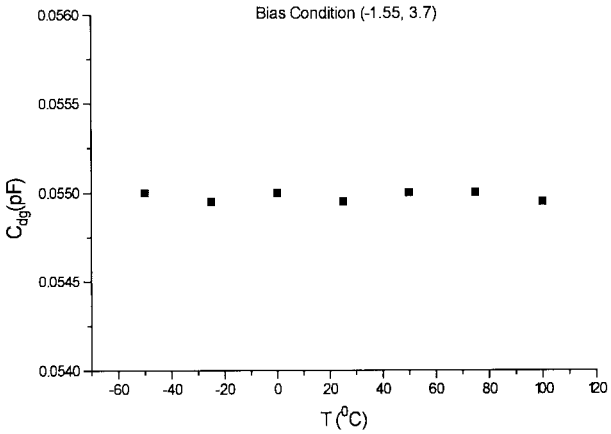

Fig. 9. $C_{\rm dg}$ as a function of temperature.

B. The Effect of Temperature

A comparison of the experimental *I–V* characteristics measured at room temperature and at temperatures below zero shows large differences as reported in [7], [8]. Such differences have also been observed for the active device used in this paper within the temperature range of −50 °C–100 °C. These measurements suggest the importance of temperature effects on the C-class amplifier characterization.

To characterize the temperature performance dependency of the NE71083, the test fixture was attached to a solid aluminum block and its temperature controlled with a proportional integral derivative temperature controller (PID). Short semirigid stainless-steel cables are used for thermal transitions between the block and the vector network analyzer (VNA). These short cables can handle the temperature gradient without significant change of their electrical characteristics. Therefore, the same TRL calibration employed in S-parameter measurements at room temperature can be used for other temperatures.

Fig. 5 shows *I–V* characteristics measured under three different temperature conditions, 100 °C, 25 °C, and −50 °C. For a value higher than the room temperature, the slopes of *I–V* characteristics increase as shown in Fig. 5 when $V_{\rm gs}$ is well under the pinch-off value and $V_{\rm ds}$ is within the saturation region. When the active device is cooled below 0 °C, poor pinch-off characteristics are obtained for $V_{\rm ds}$ higher than 3.6 V and $V_{\rm gs}$ below to −1 V as shown in Fig. 5. Similar behavior of the pinch-off characteristics has already been observed for NE71083 at cryogenic temperatures in [9]. These changes are very significant for the C-class active device operation being $V_{\rm gs} < -1.1$ V and $V_{\rm ds} > 3.6$ V at −50 °C, in which an increase of g_m is observed.

Similar behavior for g_m is observed from the experimental S-parameters' measurements performed over the same temperature range for the different bias conditions. The equivalent circuit elements' extraction method is similar to the one used at room temperature. The effect of temperature over each one of the elements is obtained from the small-signal model at each temperature value. The elements with a more significant dependency with temperature are g_m, $g_{\rm ds}$, and $C_{\rm ds}$ as shown in Figs. 6–8 for $V_{\rm gs} = -1.55$ V and $V_{\rm ds} = 3.7$ V. As observed in Fig. 6, the value of g_m changes significantly from 0 °C to −50 °C with an increment of almost 400%.

For the particular device used in this work, Figs. 7 and 8 show that a linear regression is a good fit for both $g_{\rm ds}(T)$ and $C_{\rm ds}(T)$. A different fitting may be needed if another active device is used [10].

The rest of the elements can be constrained to a constant value at each particular bias condition as shown in Figs. 9 and 10.

For large signal analysis only $g_{\rm ds}$, g_m ,$C_{\rm gs}$, and C_{gd} will be considered bias dependent. The remaining elements τ,

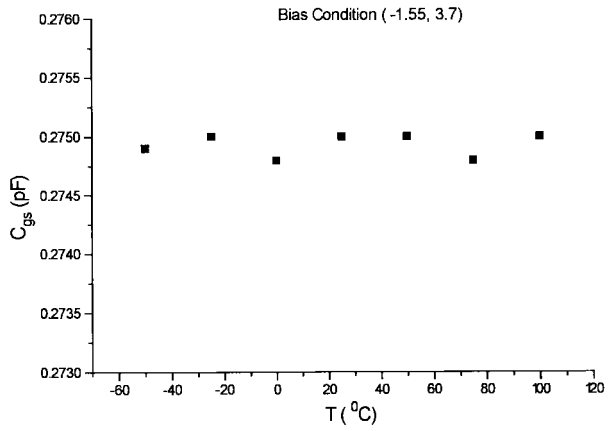

Fig. 10. $C_{\rm gs}$ as a function of temperature.

$C_{\rm ds}$, $R_{\rm GS}$, and the parasitic elements are considered to have constant values [11], [12].

III. Theoretical Analysis of a 4-Ghz Amplifier

The model obtained earlier for the NE71083 is now used as the active device of a 4-GHz C-class power amplifier. The nonlinear analysis is performed using the describing function technique. The consideration of the bias dependency of the equivalent circuit's elements allows one to determine the optimum bias conditions in C-class for maximum gain.

For this analysis, the describing function characterization of the RF-power transistor is used assuming sinusoidal components for the terminal currents.

In order to apply the described functions, it is necessary to obtain the expressions for the mean-values and the different harmonic components of the transistor terminal voltages.

According to the model shown in Fig. 11, and considering the drain and gate currents given by

$$I_d = I_{d_0} + I_{d_1}\cos(\varphi - \varphi_d) \tag{3}$$

$$I_g = I_{g_0} + I_{g_1}\cos(\varphi - \varphi_g) \tag{4}$$

the transistor terminal voltage components V_s and V_t, may be resolved in the following terms (see (5) and (6) at the bottom of the page).

The contributions to the terminal voltages from the linear elements are obtained from straightforward circuit analysis and Fourier series calculations. The contributions V_d and V_g from the nonlinear elements are calculated as a function of the total charge Q_d and Q_g, respectively, obtained from the experimental drain and gate C–V characteristics. For the device used in this paper, a parabolic approximation gives an excellent fit for both charge–voltage relationships.

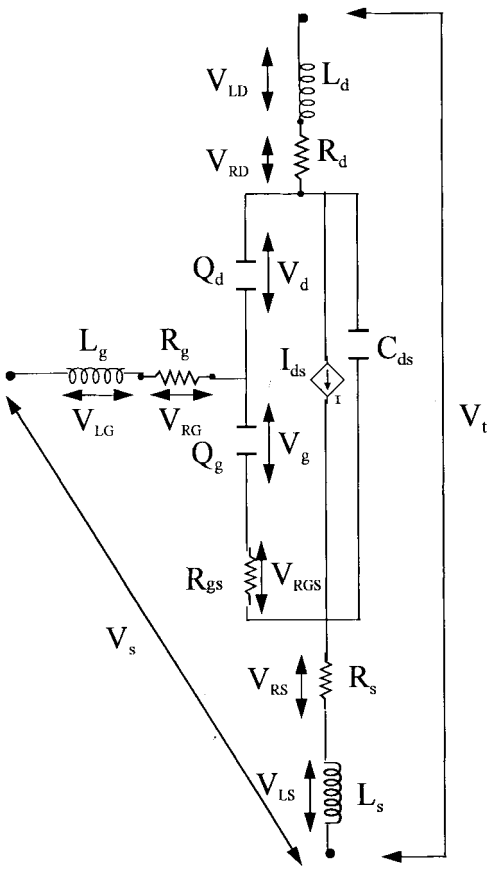

Fig. 11. Active device equivalent circuit.

Once the device terminal currents and voltages are known, the describing functions are then calculated as the nonlinear impedances at each frequency component.

The complete amplifier is represented by a system of nonlinear equations that must be solved simultaneously for the unknown variables: terminal currents' waveform parameters and bias conditions $V_{\rm ds}$ and $V_{\rm gs}$.

For computational purposes, the system of nonlinear equations is divided into four subsystems as

$$S = \{S_{\rm bias}, S_{\rm in}, S_{\rm out}, S_{\rm opt}\}, \tag{7}$$

$S_{\rm bias}$ is related to the bias circuit and is given by

$$V_{s_0} - V_{\rm GG} = 0 \tag{8}$$

$$V_{t_0} - V_{\rm DD} = 0 \tag{9}$$

where $V_{\rm GG}$ and $V_{\rm DD}$ correspond to the gate and drain bias supply voltages, respectively.

$$\left.\begin{aligned} V_{s_0} &= V_{G_0} + V_{\rm RS_0} + V_{\rm RGS_0} \\ V_{t_0} &= V_{G_0} + V_{D_0} + V_{\rm RS_0} + V_{\rm RD_0} + V_{\rm RGS_0} \end{aligned}\right\}\text{mean values} \tag{5}$$

$$\left.\begin{aligned} \vec{V}_{s_1} &= \vec{V}_{\rm LG_1} + \vec{V}_{\rm RG_1} + \vec{V}_{G_1} + \vec{V}_{\rm RGS_1} + \vec{V}_{\rm LS_1} + \vec{V}_{\rm RS_1} \\ \vec{V}_{t_1} &= \vec{V}_{\rm RS_1} + \vec{V}_{\rm LS_1} + \vec{V}_{\rm RGS_1} + \vec{V}_{G_1} + \vec{V}_{D_1} + \vec{V}_{\rm RD_1} + \vec{V}_{\rm LD_1} \end{aligned}\right\}\text{harmonic components} \tag{6}$$

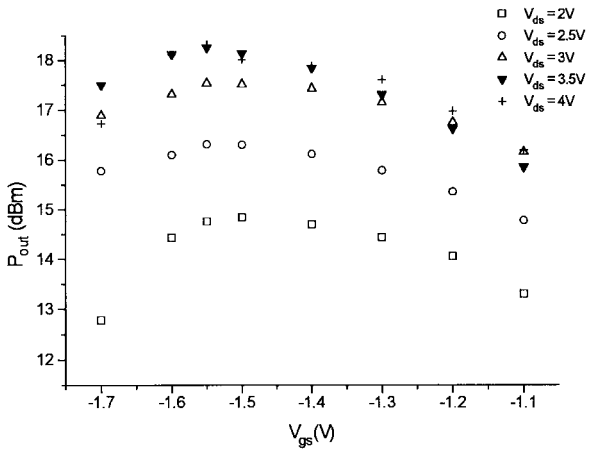

Fig. 12. Output power as a function of $V_{\rm gs}$ for different $V_{\rm ds}$ ($P_{\rm in} = 9$ dBm).

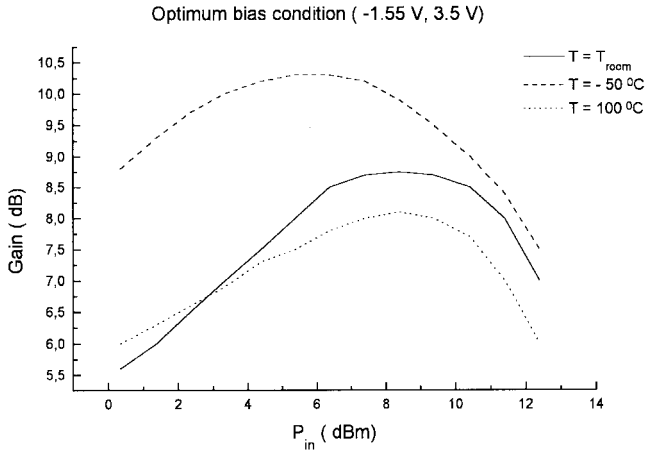

Fig. 13. Amplifier gain as a function of input power level at different temperatures.

$S_{\rm in}$ and $S_{\rm out}$ include the input and output matching networks and are given by

$$\vec{V}_{s_1} + Z_s \vec{I}_{g_1} = 0 \tag{10}$$

$$\vec{V}_{t_1} + Z_l \vec{I}_{d_1} = 0 \tag{11}$$

and finally, $S_{\rm opt}$ is the set of equations that provides the optimum bias conditions for maximum gain. This condition is given by

$$\frac{\partial P_{\rm out}}{\partial V_{\rm ds}} = 0 \tag{12}$$

$$\frac{\partial P_{\rm out}}{\partial V_{\rm gs}} = 0. \tag{13}$$

Equations (12) and (13) are only considered when the optimum bias conditions are calculated, but they are not included when the total system is solved for a particular bias condition.

Having found a solution to (7), different quantities like output power, transistor impedances, and efficiency may be directly calculated from the results. Fig. 12 shows the amplifier output power for different $V_{\rm ds}$ and $V_{\rm gs}$ conditions. A maximum output power of 18 dBm at 4 GHz with a corresponding power gain of 9 dB is obtained for the particular values of $V_{\rm ds} = 3.5$ V and $V_{\rm gs} = -1.55$ V provided by the solution of the system of nonlinear equations.

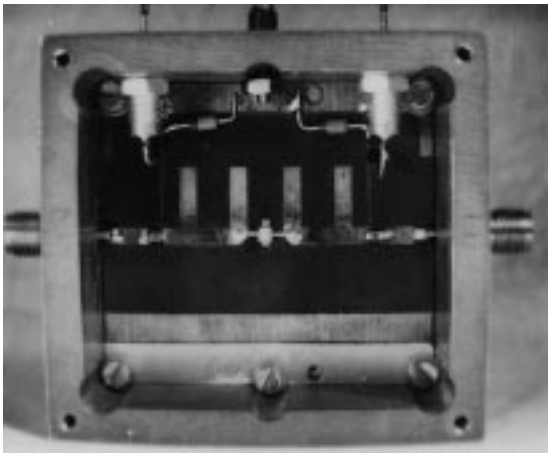

Fig. 14. Photograph of the 4-GHz amplifier designed using transistor NE71083.

Once the active device model has been determined at each temperature and for each bias condition, it is now possible to study the amplifier performance for each temperature and bias point. The values of $V_{\rm ds}$ and $V_{\rm gs}$ are fixed and then the nonlinear system of (7) is solved for each temperature value within the range of -50 °C to 100 °C. Fig. 13 shows the amplifier gain obtained at three different temperatures for the optimum bias condition as a function of input power. As is observed, an increase of gain is obtained at lower temperatures. Also, the gain is not as dramatically reduced as is observed at higher temperatures for low-input power levels.

IV. Experimental Results

In order to confirm the validity of the bias and temperature device model dependencies a 4-GHz experimental amplifier has been designed. The synthesis on the microstrip of the input and output active device impedances, provided by the describing function technique, is carried out by using MWAVE [13].

A photograph of the 4-GHz amplifier designed using transistor NE71083 is shown in Fig. 14. A maximum gain of 8 dB was obtained at 4.3 GHz for the biasing conditions $V_{\rm gs} = -1.55$ V and $V_{\rm ds} = 3.5$ V. These values are in excellent agreement with the theoretical results obtained in Section III. Fig. 15 shows the experimental amplifier gain as a function of the input power for different bias conditions.

The optimum bias condition, ($-$1.55,3.5), provide the maximum gain value as well as the widest region where the gain is constant. Fig. 16 shows a comparison between theoretical (continuous graph) and experimental (dots) amplifier gain as a function of bias conditions. As shown, the maximum value in both graphs is located at ($-$1.55,3.5) and all experimental values are consistently 1 dB lower than the corresponding theoretical values. This is due to the losses of the input and output matching networks as well as the decoupling capacitors which have not been considered in the theoretical analysis.

The experimental study of the amplifier RF performance as a function of temperature is performed by using an iden-

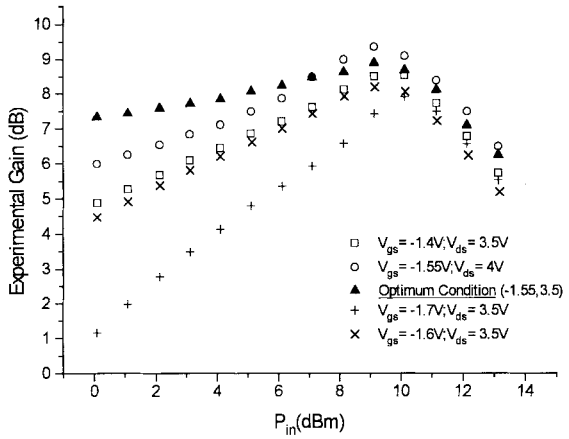

Fig. 15. Experimental gain as a function of input power for different bias conditions at room temperature.

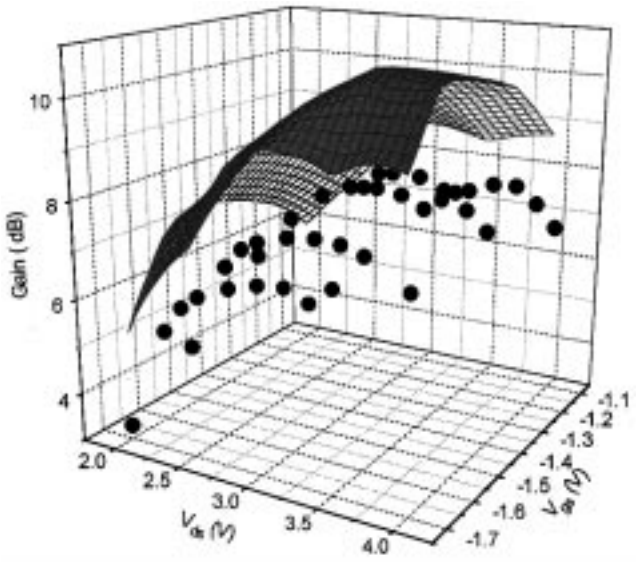

Fig. 16. Theoretical and experimental amplifier gain as a function of the bias voltages at room temperature ($P_{\rm in} = 9$ dBm).

tical setup as mentioned in Section II for the experimental characterization of the device. The amplifier gain is measured for each particular bias condition and for each temperature within the range of −50 °C to 100 °C. Fig. 17 shows the amplifier gain as a function of the input power for different temperatures for the bias conditions (−1.55,3.5), corresponding to maximum gain at room temperature, and (−1.4,3.5). As observed, a higher amplifier gain (11 dB) is obtained for the optimum bias condition at the lowest temperature −50 °C. It has also been observed that the maximum input power before saturation has a lower value although the region where the gain is constant has increased. For the other bias condition (−1.4,3.5), the variation of the amplifier gain is not so significant and the amplifier is saturated for very small values of input power.

Also, for the optimum bias condition, the increase in the amplifier gain for temperatures below the room temperature is clearly observed with the steepest increase corresponding to temperatures below 0 °C. At temperatures higher than room

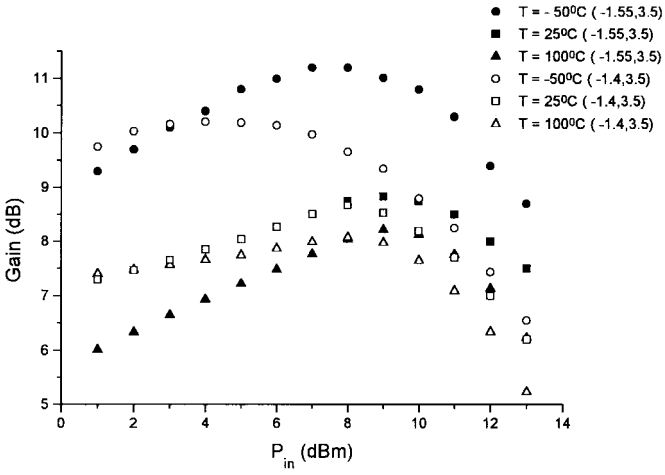

Fig. 17. Experimental gain versus input power for different temperatures at (−1.55,3.5) and (−1.4,3.5).

temperature, the amplifier gain has a value very similar to the value at room temperature. The different graphs corresponding to the different input power values show the variation of the amplifier saturation level. It is also observed that at temperatures below 0 °C, the maximum amplifier gain can be obtained for a lower input power level (7 dBm) than what corresponds to room temperature (9 dBm). For higher temperature values, however, the maximum gain value corresponds to the input power value at room temperature. For the other bias conditions, (−1.4,3.5), the increase in the amplifier gain is considerably reduced and the amplifier saturation input power value is the lowest possible, as shown in Fig. 17.

V. Conclusion

A complete device model which is bias and temperature dependent, has been derived for a MESFET transistor. The advantage of this model is that the equivalent circuit parameters can be determined from the experimental active device characterization without requiring optimization.

A MESFET C-class amplifier has been designed, analyzed, and optimized by using the model previously obtained. The nonlinear analysis of the amplifier is performed using the describing function technique. This approach makes the appropriate design of the input and output matching networks possible, as well as the determination of the optimum bias conditions for maximum gain and the amplifier performance as a function of temperature in C-class.

The experimental results of the amplifier shows the validity of the model to characterize bias and temperature behavior of the active device and the suitability of the describing function technique for the nonlinear analysis and optimization of the complete amplifier.

References

[1] F. Filicori, V. A. Monaco, and C. Naldi, "Simulation and design of microwave class-C amplifiers through harmonic analysis," *IEEE Trans. Microwave Theory Tech.*, vol. MTT-27, pp. 1043–1051, Dec. 1979.

[2] H. Fukui, "Determination of the basic device parameters of GaAs MESFET," *Bell Syst.Tech. J.*, vol. 58, no. 3, pp. 711–797, Mar. 1979.

[3] F. Diamant and M. Laviron, "Measurement of the extrinsic series elements of a microwave MESFET under zero current condition," in *Proc. 12th European Microwave Conf.*, Helsinki, Finland, Sept. 1982, pp. 451–456.
[4] G. Dambrine, A. Cappy, F. Heliodore, and E. Playez, "A new method for determining the FET small-signal equivalent circuit," *IEEE Trans. Microwave Theory Tech.*, vol. 36, pp. 1151–1159, July 1988.
[5] R. B. Marks, "A multiline method of network analyzer calibration," *IEEE Trans. Microwave Theory Tech.*, vol. 39, pp. 1205–1215, July 1991.
[6] J. Rodriguez-Tellez, K. A. Merher, O. M. Conde Portilla, and J. C. Luengo Patrocinio, "A highly accurate microwave nonlinear MESFET model," *Microwave J.*, pp. 280–285, May 1993.
[7] P. C. Canfield, S. C. F. Lam, and D. J. Allstot, "Modeling of frequency and temperature effects in GaAs MESFET's," *IEEE J. Solid-State Circuits*, vol. 25, pp. 299–306, Feb. 1990.
[8] L. Selmi and B. Ricco, "Modeling temperature effects of the DC I–V characteristics of GaAs MESFET's," *IEEE Trans. Electron Devices*, vol. 40, pp. 273–277, Feb. 1993.
[9] M. W. Pospieszalski, S. Weinreb, R. D. Norrod, and R. Harris, "FET's and HEMT's at cryogenic temperatures, their properties and use in low-noise amplifiers," *IEEE Trans. Microwave Theory Tech.*, vol. 36, pp. 552–560, Mar. 1988.
[10] S. M. Lardizabal, A. S. Fernandez, and L. P. Dunleavy, "Temperature dependent modeling of gallium arsenide MESFET's," *IEEE Trans. Microwave Theory Tech.*, vol. 44, pp. 357–363, Mar. 1996.
[11] A. Madjar and F. J. Rosenbaum, "A large-signal model for the GaAs MESFET," *IEEE Trans. Microwave Theory Tech.*, vol. MTT-29, pp. 781–788, Aug. 1981.
[12] M. Golio, *Microwave MESFET's and HEMT's*. Norwood, MA: Artech House, 1991.
[13] J. L. Sebastián and J. M. Miranda, "MWAVE 2: A tool for microwave amplifier design," in *Proc. 23rd European Microwave Conf.*, Madrid, Spain, Sept. 1993, pp. 1009–1011.

Sagrario Muñoz received the M.Sc. (speciality in electronics) and Ph.D. degrees, both in physics, from Universidad Complutense de Madrid, Madrid, Spain, in 1988 and 1996, respectively.

Since 1992, she has worked as an Academic Assistant at the Facultad de Físicas, Universidad Complutense de Madrid. Her present research activities are in the area of MESFET's and HEMT's characterization and microwave circuit design.

Jose L. Sebastián was born in Zaragoza, Spain, in 1950. He received the Licenciatura and Grado de Licenciado degrees, both in physics, from Universidad Complutense de Madrid, Madrid, Spain, and the Ph.D. degree in physics from the University of Surrey, U.K., in 1973, 1974, and 1977, respectively.

In 1977, he joined the Universidad Complutense as a Reader, and in 1983 he was appointed full Professor of Electricity and Magnetism. He has been involved in RF device characterization and acousto-optic devices. He is currently working in nonlinear characteristics of microwave devices and computer simulation of new microwave circuits.

Dr. Franco is presently the Chairman of the Spanish URSI Committee.

Juan D. Gallego (M'91) was born in Madrid, Spain, on June 4, 1960. He received the Licenciado degree (with honors), and the Ph.D. degree, both in physics, from Universidad Complutense de Madrid, Madrid, Spain, in 1984 and 1992, respectively.

In 1985 he joined Centro Astronómico de Yebes (Observatorio Astronómico Nacional), Guadalajara, Spain, where he has been involved in the development of low-noise microwave and millimeter-wave receivers for radio-astronomy applications. In 1989 he spent one year at the National Radio Astronomy Observatory, Charlottesville, VA, working on the development of cryogenic HEMT amplifiers. His current research areas are microwave measurement techniques, low-phase noise oscillators, and ultra-low-noise cryogenic HEMT amplifiers.